GEOLOGICAL SURVEY OF CANADA
OPEN FILE 7852

Targeted Geoscience Initiative 4: Contributions to the Understanding of Precambrian Lode Gold Deposits and Implications for Exploration

Setting, age, and hydrothermal footprint of the emerging Meliadine gold district, Nunavut

Christopher J.M. Lawley[1], Benoît Dubé[2], Patrick Mercier-Langevin[2], Vicki J. McNicoll[1], Robert A. Creaser[3], Sally J. Pehrsson[1], Sébastien Castonguay[1], Jean-Claude Blais[4], Marjorie Simard[4], William J. Davis[1], and Simon E. Jackson[1]

[1]Geological Survey of Canada, Ottawa, Ontario
[2]Geological Survey of Canada, Québec, Quebec
[3]University of Alberta, Edmonton
[4]Agnico Eagle Mines Ltd., Val D'Or, Quebec

2015

This publication is available for free download through GEOSCAN (http://geoscan.nrcan.gc.ca/)

Recommended citation

Lawley, C.J.M., Dubé, B., Mercier-Langevin, P., McNicoll, V.J., Creaser, R.A., Pehrsson, S.J., Castonguay, S., Blais, J.-C., Simard, M., Davis, W.J., and Jackson, S.E., 2015. Setting, age, and hydrothermal footprint of the emerging Meliadine gold district, Nunavut, *In:* Targeted Geoscience Initiative 4: Contributions to the Understanding of Precambrian Lode Gold Deposits and Implications for Exploration, (ed.) B. Dubé and P. Mercier-Langevin; Geological Survey of Canada, Open File 7852, p. 99–111.

Publications in this series have not been edited; they are released as submitted by the author.

Contribution to the Geological Survey of Canada's Targeted Geoscience Initiative 4 (TGI-4) Program (2010–2015)

TABLE OF CONTENTS

Setting, age, and hydrothermal footprint of the emerging Meliadine gold district, Nunavut

Christopher J.M. Lawley[1]*, Benoît Dubé[2], Patrick Mercier-Langevin[2], Vicki J. McNicoll[1], Robert A. Creaser[3], Sally J. Pehrsson[1], Sébastien Castonguay[1], Jean-Claude Blais[4], Marjorie Simard[4], William J. Davis[1], and Simon E. Jackson[1]

[1]Geological Survey of Canada, 601 Booth Street, Ottawa, Ontario K1A 0E8
[2]Geological Survey of Canada, 490 rue de la Couronne, Québec, Quebec G1K 9A9
[3]Department of Earth and Atmospheric Sciences, 1-26 Earth Sciences Building, University of Alberta, Edmonton, Alberta T6G 2E3
[4]Agnico Eagle Mines Ltd, 765 Chemin de la mine Goldex, Val D'Or, Quebec J9P 4N9
*Corresponding author's e-mail: clawley@nrcan.gc.ca

ABSTRACT

The Meliadine gold district comprises a combination of orogenic greenstone- and BIF-hosted gold mineralization. The largest gold deposits (Tiriganiaq, Wesmeg, Normeg, F Zone, Pump, Discovery, and Wolf) are cospatial with the northwest-trending Pyke Fault and its inferred east-trending splays, which cut amphibolite- to greenschist-facies rocks within the Rankin Inlet greenstone belt. New U-Pb detrital zircon ages suggest that turbiditic and mafic volcanic host rocks at Tiriganiaq were deposited ≤2.66 Ga. In contrast, a polymictic conglomerate south of the Pyke Fault, which is not known to host gold, yielded Paleoproterozoic U-Pb detrital zircons and was deposited at ≤2.50 Ga. These new ages confirm that the Rankin Inlet greenstone belt comprises intercalated Archean to Paleoproterozoic supracrustal successions. Deformed Paleoproterozoic conglomerates suggest that the Archean to Proterozoic Rankin Inlet stratigraphy was reworked during the Trans-Hudson Orogeny (1.9–1.8 Ga).

Gold in the district is associated with hydrothermally altered and sulphidized BIF and fault-fill quartz (± ankerite) veins. Hydrothermal alteration and pathfinder element enrichment (As-Te-Bi-Sb) can be mapped following a multivariate and probabilistic approach for 10s to 100s of meters beyond BIF-hosted replacement-style mineralization. Coarse-grained and idioblastic arsenopyrite crystals occur within and at the margins of folded quartz (± ankerite) veins and are also a good visual gold indicator. Gold is paragenetically late and occurs at arsenopyrite grain boundaries and/or as fracture fills. Clusters of gold inclusions coincide with recrystallized and sieve-textured arsenopyrite domains. These microtextures suggest that sulphide recrystallization liberated gold that was redistributed, at least locally, into low-strain microtextural sites along with other precious- and base-metals during a late fluid-assisted and deformation/metamorphic-driven remobilization. We propose that remobilization was concurrent with the growth of xenotime at ca. 1.86 Ga (new U-Pb ages), which postdates arsenopyrite and occurs together with gold in low-strain micro textural sites. New Re-Os arsenopyrite model ages range from 2.3 to 1.8 Ga and document a hitherto unrecognized pre-1.86 Ga hydrothermal and sulphide history. The range of Re-Os model ages tends to support partial open-system behaviour and/or mixing of disparate arsenopyrite generations that are evident from microtextures and in situ element mapping. Replicate analyses of the two most Re-rich and homogeneous arsenopyrite samples yield Re-Os model ages at ca. 2.27 and 1.90 Ga. We speculate that gold at the Meliadine gold district was initially introduced at 2.27 Ga and/or 1.90 Ga along with arsenopyrite and was subsequently remobilized, coupled with arsenopyrite recrystallization, during the Trans-Hudson Orogeny at 1.86–1.85 Ga.

INTRODUCTION

The Meliadine Gold District (MGD) research activity represents one component of the Banded Iron Formation (BIF)-hosted deposits subproject within the Lode Gold project of the Targeted Geoscience Initiative (TGI)-4 program (Dubé et al., 2011). Research at the MGD is conducted in close collaboration with Agnico-Eagle Mines Ltd. and focuses on further defining the setting, age, and hydrothermal footprint at this emerging gold district (2.8 Moz contained gold within an indicated and inferred resource of 5.8 Moz; www.agncioeagle.com). Prior to this study, the metallogenic model at the MGD emphasized a relatively late gold history (Carpenter and Duke, 2004;

Lawley, C.J.M., Dubé, B., Mercier-Langevin, P., McNicoll, V.J., Creaser, R.A., Pehrsson, S.J., Castonguay, S., Blais, J.-C., Simard, M., Davis, W.J., and Jackson, S.E., 2015. Setting, age, and hydrothermal footprint of the emerging Meliadine gold district, Nunavut, *In:* Targeted Geoscience Initiative 4: Contributions to the Understanding of Precambrian Lode Gold Deposits and Implications for Exploration, (ed.) B. Dubé and P. Mercier-Langevin; Geological Survey of Canada, Open File 7852, p. 99–111.

Carpenter et al., 2005). The model was based, in large part, on hydrothermal monazite U-Pb ages (1.85 Ga) that were interpreted to be cogenetic with gold at the Tiriganiaq deposit and correlative with the Trans-Hudson Orogeny (THO; 1.9–1.8 Ga; Carpenter et al., 2005). The apparent link between gold and late west-trending shear zones was taken as further evidence of late gold introduction at the MGD (Carpenter and Duke, 2004). However, the gold fertility of pre-THO structures was undocumented. Published geochronology for the Rankin Inlet greenstone belt was also limited to U-Pb zircon dating of a felsic band (originally interpreted as a porphyritic rhyolite) intercalated with mafic volcanic rocks at ca. 2.66 Ga (Tella et al., 1996). This sample was collected south of the major gold-bearing structure in the MGD (i.e. the Pyke Fault; Fig 1) and thus the ages of the rocks hosting the gold deposits remained speculative.

In this contribution, we briefly outline TGI-4 field and laboratory results that further constrain the setting, age, and hydrothermal footprint at the MGD. Critically, we document a hitherto unrecognized pre-1.85 Ga hydrothermal history at the MGD. The implications of 'early' auriferous hydrothermal activity to ongoing mineral exploration are also briefly discussed.

RESULTS AND DATA ANALYSIS

Setting

Regional Setting

West of Hudson Bay, the Western Churchill Province (WCP) is broadly divided into the Rae and Hearne cratons separated by the cryptic and polyorogenic Snowbird Tectonic Zone (Hoffman, 1988). However, more recent work has further subdivided the WCP into the Central Hearne subdomain and the Chesterfield Block (Berman et al., 2007, 2013; Pehrsson et al., 2013a, b). These authors placed the MGD at the boundary between the Central Hearne and the Chesterfield Block. Cratonic boundaries are widely recognized as first-order controls on the distribution of gold deposits and represent significant exploration targets.

Host Rocks

The MGD host rocks were originally assigned to the Rankin Inlet Group (Bannatyne, 1958) and later referred to as the Rankin Inlet greenstone belt (e.g. Aspler and Chiarenzelli, 1996). The district is dominated by volcanic rocks (basalt, andesite, and rare rhyolite), interflow volcaniclastic rocks and, more rarely, graded-bedded greywacke-siltstone-mudstone successions, quartzite and BIF. Metamorphosed and deformed granitic to tonalitic intrusions are intercalated with these supracrustal rock packages. Mafic volcanic and volcaniclastic rocks, known locally as the Wesmeg formation, represent the two main rock types at Wesmeg, Normeg, F Zone, and Pump and constitute the footwall at Tiriganiaq (Figs. 1–3). Graded-bedded greywacke-siltstone-mudstone rock assemblages are interpreted as turbidite sucessions and are known locally as the Sam and Tiriganiaq formations (Fig. 3a, b; Carpenter and Duke, 2004). Turbidite sequences comprise the hanging wall at Tiriganiaq and represent the dominant host rock at Discovery. Algoma-type BIF is interbedded with mafic volcanic and volcaniclastic rocks (i.e. oxide facies; Wesmeg, Pump, and F Zone deposits) and a greywacke-siltstone-chloritic mudstone rock assemblage (i.e. silicate facies; Tiriganiaq and Discovery deposits). Oxide-facies BIF is significantly more chert-rich than silicate-facies BIF.

Structure

The structural history of the MGD is broken into four distinct phases of deformation (Fig. 3a; Carpenter and Duke, 2004; Carpenter et al., 2005). The earliest recognizable deformation event (D_1) lacks a clear cleavage although it is linked to bedding-parallel thrusting and folding that may have resulted in the initial juxtaposition of volcanic-sedimentary packages (Tella et al., 1992; Carpenter and Duke, 2004). The largest gold deposits occur along the Pyke Fault and its associated splays (e.g. Lower Fault at Tiriganiaq; Figs. 1, 2). Carpenter and Duke (2004) have proposed that these faults may have developed during this earliest deformation event; however, the timing and nature of D_1, and especially its relationship to gold, remain poorly constrained.

A second deformation increment (D_2) resulted in bedding-parallel folding and thrusting and a penetrative northwest-trending foliation (S_2: 285/59; Carpenter and Duke 2004). This deformation event was likely coupled with shearing and reactivation of the Pyke Fault and associated west-trending fault splays (e.g. Lower Fault; Carpenter and Duke, 2004). TGI-4 fieldwork along the newly constructed all-season road between the town of Rankin Inlet and the Meliadine exploration camp identified that recumbent and isoclinals folds (F_1?) were refolded during D_2 to produce the dominant map pattern south of the Pyke Fault (Fig. 1; akin to Fig. 2 of Tella et al., 1992).

The dominant regional foliation (S_2) predates a west-trending cleavage (S_3) that is best developed within turbidite and represents the dominant fabric geometry at Tiriganiaq. Northeast-plunging regional- to outcrop-scale Z-shaped folding may have developed during this D_3 event (Carpenter and Duke, 2004). The relationship between asymmetric folding and D_3 reactivation of the Pyke and Lower faults and gold forms the basis for the late gold metallogenic model at the MGD (Carpenter and Duke, 2004; Carpenter et al., 2005).

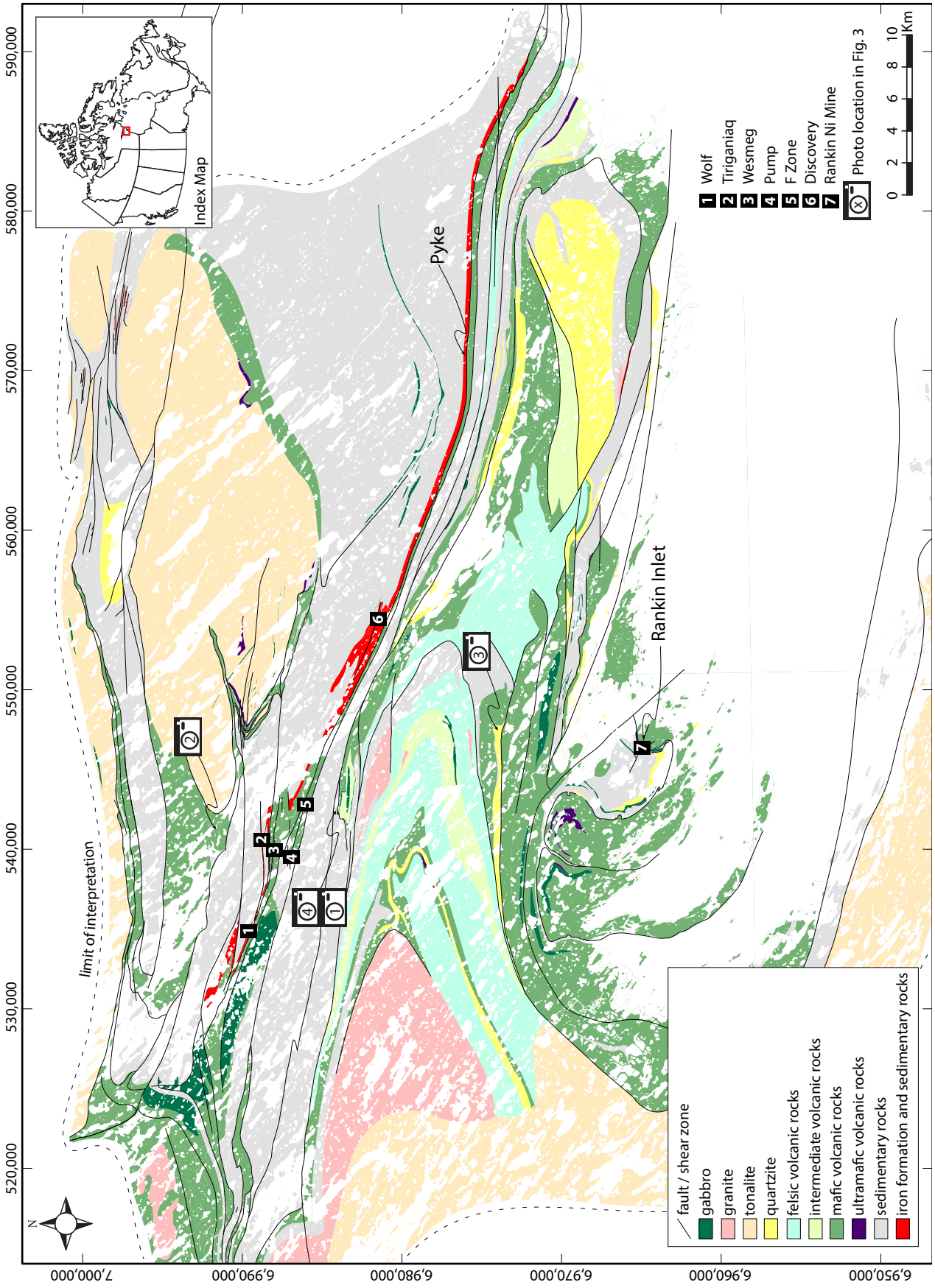

Figure 1. Local Meliadine gold district geology map (courtesy of Agnico-Eagles Mines Ltd.). The Pyke Fault, gold deposits, and the former Rankin Nickel Mine are shown for reference. Camera symbols correspond to outcrop photos presented in Figure 3.

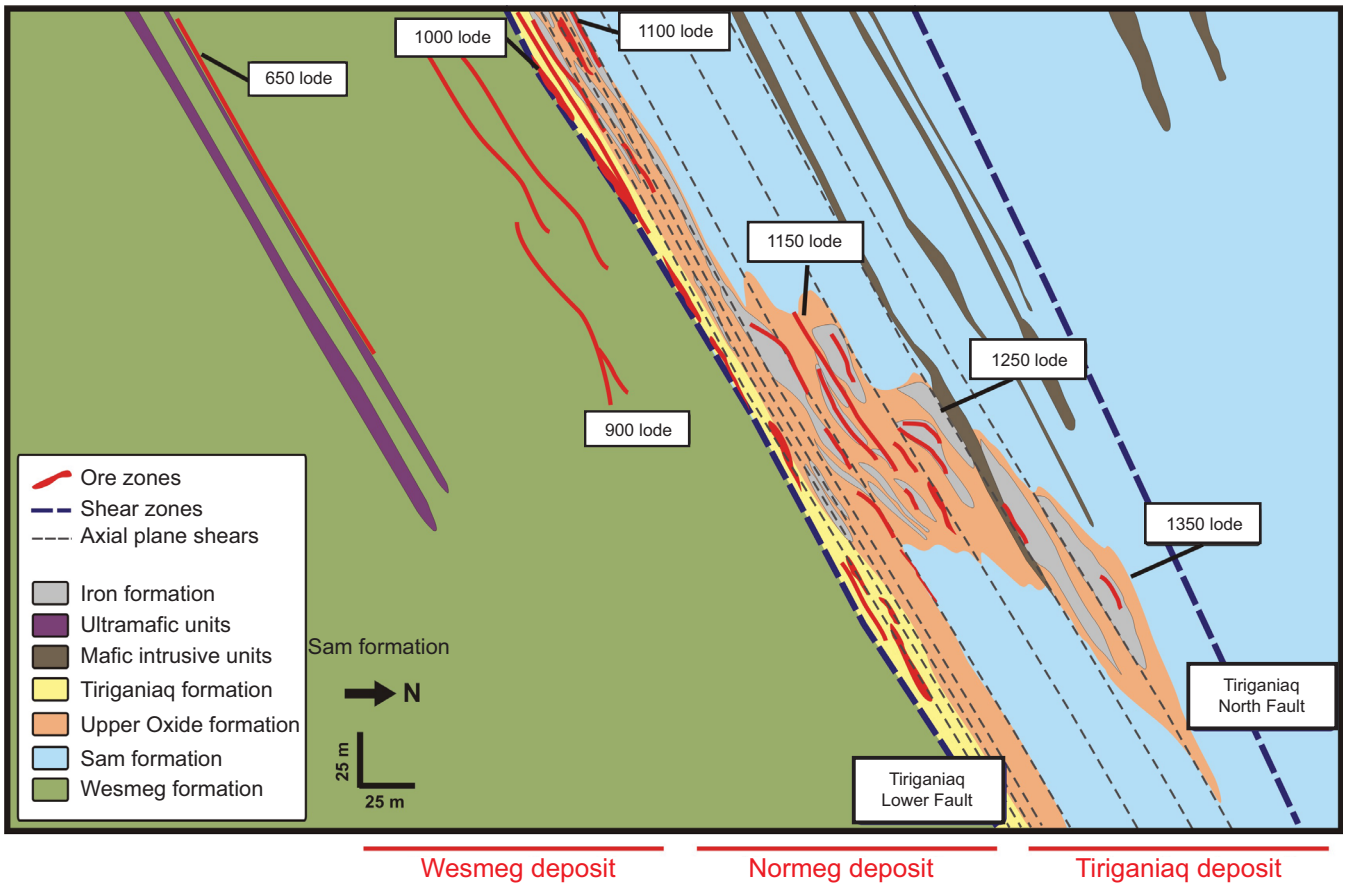

Figure 2. Simplified cross section showing the Tiriganiaq, Normeg, and Wesmeg deposits (courtesy of Agnico-Eagles Mines Ltd.). Section highlights folded BIF and turbidite (Sam and Upper Oxide formations) in the hanging wall at Tiriganiaq. Ore zones and BIF are transposed and axial planar to folds and are also parallel to the Lower Fault. Gold-rich intervals at Wesmeg locally occur along ultramafic and mafic volcanic (i.e. Wesmeg Formation) contacts.

At Tiriganiaq, auriferous quartz (± ankerite) veins are tightly folded, boudinaged, and transposed parallel to the main fabric (265/65N; Fig. 4a–d), which could represent (1) a locally penetrative S_3 fabric, developed subparallel to the west-trending and steeply dipping Lower Fault (Carpenter and Duke, 2004; Carpenter et al., 2005); (2) the main regional foliation (S_2) transposed into a west-trending orientation by D_3 strain (Miller et al., 1995); or (3) a composite S_2-S_3 fabric. The dearth of clear S_2-S_3 relationships underground at Tiriganiaq makes distinguishing between these possibilities equivocal. However, S_{main} is axial planar to tight folds in turbidite (Fig. 3b) and BIF, which is unlike S_3-S_0 relationships distal to D_3 shear zones (Fig. 3a). This relationship likely reflects transposed bedding adjacent to D_3 shear zones (e.g. Lower Fault), but could also suggest that the main deposit fabric at Tiriganiaq represents the dominant regional foliation (S_2) transposed into a west-trending orientation.

Asymmetric porphyroclasts and boudinaged quartz veins, coupled with the geometry of en echelon extension quartz (± ankerite) veins in the Tiriganiaq deposit structural hanging wall, suggests a component of reverse sense of motion during the main phase of deformation. This reverse component of motion postdates, or was synchronous with, auriferous quartz (± ankerite) veining (Fig. 4a–d). The main quartz vein at Tiriganiaq occurs within the Lower Fault and is interpreted as a fault-fill vein type (Fig. 4a, c; i.e., laminated appearance; included slivers of mylonitized wall rock; stylolites). Attendant flat-dipping extensional veins are also tightly folded, transposed by the main deposit fabric, and commonly occur as rootless folds (Fig. 4a). This suggests that these fault-fill and extensional quartz-ankerite veins were emplaced in an active deformation zone and thus contrast with the post-deformational vein timing (late D_3) proposed by Carpenter et al. (2005).

The final phase of deformation, D_4, is characterized by a northwest- to north-trending crenulation cleavage (S_4) and kink bands, which are best developed in fissile turbidite and mafic volcaniclastic successions (Fig. 3a). The late crenulation cleavage is generally steeply dipping and produces a strong vertical intersection lineation on S_2 foliation planes. This final phase of deformation does not significantly modify earlier structures, is not associated with mineralization, and likely postdates the introduction of gold (Carpenter and Duke,

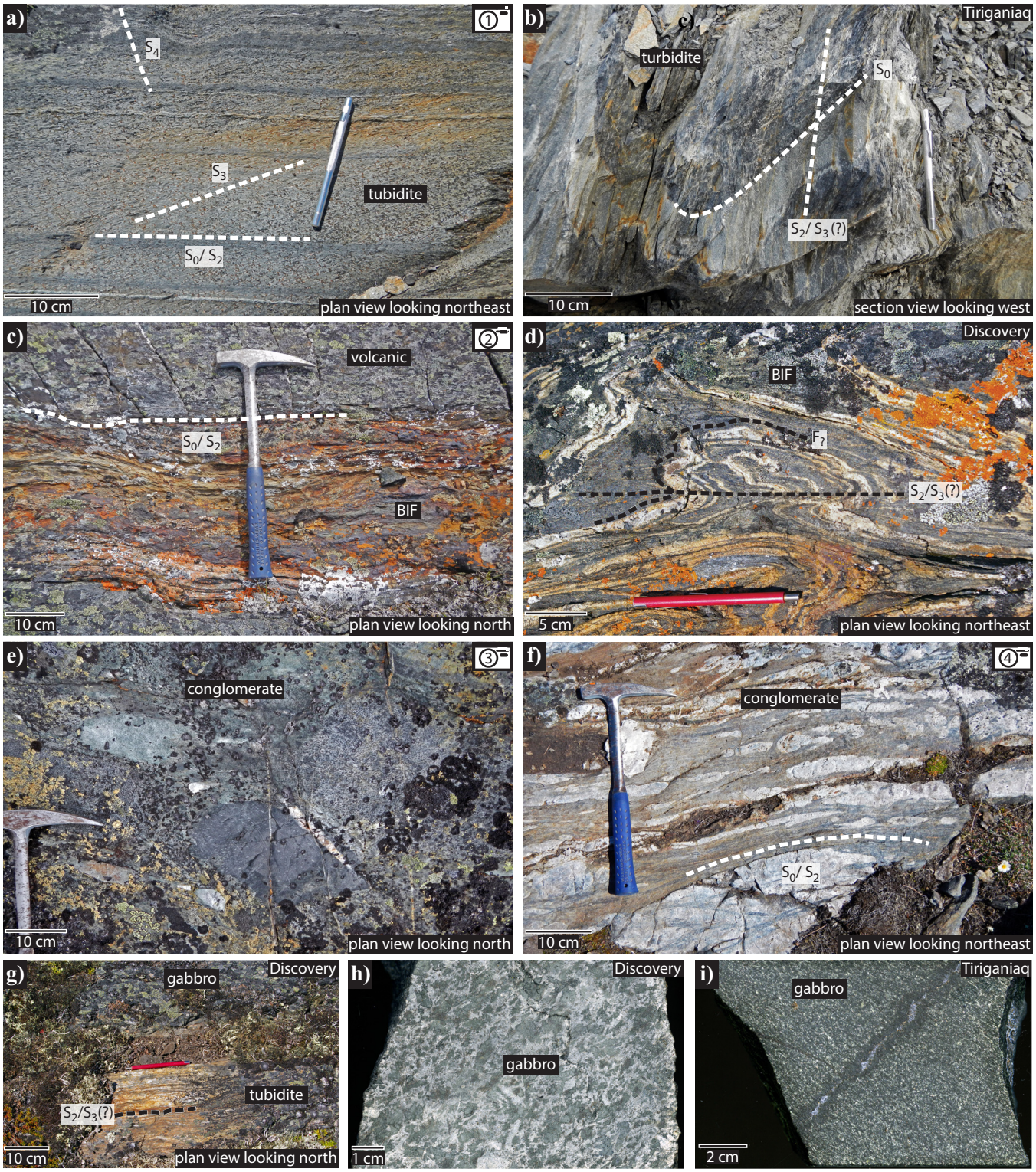

Figure 3. a) Turbidite showing three foliations (S_2–S_4) reported by Carpenter and Duke (2004). **b)** Turbidite bedding at Tiriganiaq. The main deposit fabric (S_2 or S_3) is axial planar to folded turbidite bedding at Tiriganiaq. **c)** BIF intercalated with mafic volcanic rock. **d)** Refolded BIF outcrop at Discovery. **e)** Polymictic conglomerate deposited ≤2.50 Ga. Conglomerate comprises muscovite schist, quartzite, metadiorite, and metabasalt clasts set in a siltstone matrix. **f)** Conglomerate deposited ≤2.66 Ga. The conglomerate comprises quartzite and tonalite/granodiorite clasts set in a siltstone matrix. **g–h)** A gabbroic dyke cutting the turbiditic host rocks at Discovery. The dyke is folded and transposed parallel to the main deposit fabric (S_2 or S_3). A zircon age of ca. 1.81 Ga obtained from the dyke most likely records the timing of metamorphism, or a hydrothermal event, as opposed to its emplacement age. **i)** Massive to foliated equigranular gabbroic dyke cutting turbiditic host rocks at Tiriganiaq. A U-Pb zircon crystallization age of ca. 90 Ma was obtained from this sample, significantly younger than any known magmatic activity in the Rankin Inlet region (Davis and Miller, 2001; N.B. veins were excluded prior to sample crushing).

2004). A deformed ≤2.155 Ga conglomeratic horizon south of the Pyke Fault is transposed parallel to the main regional foliation (S_2) and suggests that the Rankin Inlet Group was significantly reworked during the THO (Davis et al. 2008).

Structural Controls at the Tiriganiaq Deposit

Most of the mineralized zones (i.e. lodes) at the Tiriganiaq deposit are oriented parallel to the west-trending Lower Fault (Fig. 2), which is situated a few hundred metres to the north of the Pyke Fault (Fig. 1). These predominantly west-trending ore zones consist of folded quartz-carbonate-sulphide veins that cut sulphidized BIF and intercalated turbiditic rocks (Figs. 2, 4g). The 1100–1350 lodes are type examples of this mineralization style and extend into the Tiriganiaq hanging wall (Fig. 2). Auriferous quartz (± ankerite) veins within these lodes are predominately west- to west-southwest-trending and subparallel to the main deposit fabric at Tiriganiaq. The 1000 lode is hosted within the Lower Fault and corresponds to a wide (1–2 m) fault-fill quartz vein (Fig. 4a) that is folded, boudinaged, and transposed parallel to the main deposit fabric (Fig. 4a–d). Subordinate northwest- and north-trending quartz veins also host gold and are also folded by the main deposit fabric near the Lower Fault at Tiriganiaq. Mineralized BIF is tightly S-folded, probably during D_2, and further sheared especially along the Lower Fault, either late during D_2, and/or during D_3 dextral shearing (Fig. 2). Late movement along the Lower Fault cuts the southern limb of this S-shaped fold (Fig. 2). Two high-grade ore shoots are recognized at Tiriganiaq: (1) one ore trend plunges approximately 45º to the east and may correspond to the intersection between the main west-trending shear fabric and the axes of northeast-plunging folds (D_3?), and (2) a second ore trend plunges approximately 25º to the west, which parallels the hinge zone of the tightly S-folded BIF (Fig. 2).

Age

Regional U-Pb Zircon Geochronology

Six samples from the Rankin Inlet greenstone belt were targeted for U-Pb zircon dating (Lawley et al., in prep). Detrital zircons were analyzed from sedimentary and volcaniclastic samples using the SHRIMP (Sensitive High Resolution Ion Microprobe). Two of these samples (turbiditic hanging wall and mafic volcaniclastic footwall) host the Tiriganiaq deposit and yield detrital zircons with ages that range from 2.94 to 2.66 Ga, which suggests that both host rocks at Tiriganiaq were deposited ≤2.66 Ga (Lawley et al., in prep). A gabbroic dyke that cuts meta-turbiditic rocks at the Discovery deposit yield zircon crystals that were dated at ca. 1.81 Ga (U-Pb SHRIMP). This gabbroic dyke at Discovery (Fig. 3h; 'feather' gabbro of Carpenter and Duke, 2004) is folded and transposed parallel to the main foliation (Fig. 3g), which suggests that this fabric and the main MGD map pattern is the result of Paleoproterozoic reworking. However, zircons from this folded dyke are clearly metamict and contain significant common Pb. These zircon textures and compositions suggest that the zircon ages record the timing of metamorphism, or a hydrothermal event, rather than the crystallization age of the gabbroic dyke. A second gabbroic dyke that cuts meta-turbiditic host rocks at the Tiriganiaq deposit was dated at ca. 90 Ma (U-Pb ID-TIMS; Isotope Dilution-Thermal Ionization Mass Spectrometry; Fig. 3i). This crystallization age is significantly younger than any known Phanerozoic magmatism in the Rankin Inlet region (e.g. ca. 214 Ma kimberlite; Davis and Miller, 2001).

Two conglomerates were also dated south of the Pyke Fault. One of these samples is polymictic and

Figure 4 opposite. a) Underground photo of the 1000 lode at Tiriganiaq (photo credit to Agnico-Eagle Mines Ltd.). The main quartz vein occurs at the Lower Fault and is interpreted as a fault-fill vein. Dragging of the main fabric in the hanging wall is consistent with a reverse sense of motion postdating or synchronous with veining. Attendant extension veins are transposed and folded by Smain (S_2/S_3?). **b)** Underground photo of the 1000 lode at Tiriganiaq (photo credit to Agnico-Eagle Mines Ltd.). The main deposit fabric is parallel to transposed bedding. Auriferous quartz veins are folded and transposed. **c)** Underground wall photo at Tiriganiaq showing the high-grade 1000 lode (Smain is dipping towards the viewer). The main quartz vein is transposed, folded, and boudinaged parallel to S_{main}. **d)** Underground photo of transposed, folded, and boudinaged quartz (± ankerite) veins structurally above the 1000 lode at Tiriganiaq. **e)** Underground photo of lamprophyre dyke cutting mafic volcanic and quartz veins at Tiriganiaq. This dyke is apparently undeformed and clearly cuts S_{main}. Lamprophyre dykes in the MGD may be correlative with the 1.833 Ga Christopher Island Formation (Rainbird et al., 2006) and could suggest that the main regional foliation is ≥1.833 Ga. **f)** Core photo of a quartz vein and alteration halo at Pump. Arsenopyrite is concentrated within the vein's alteration halo along with chlorite-sericite-calcite. **g)** Core photo of a high-grade BIF interval at Tiriganiaq showing folded quartz veins and associated idioblastic arsenopyrite. **h)** Core photo of a folded quartz (± ankerite) and gold vein at Wolf. S_{main} appears axial planar to the fold. Idioblastic arsenopyrite crystals occur peripheral to the vein. **i)** Core photo of a folded quartz vein at Wesmeg. Idioblastic is concentrated within folded chloritic bands. **j)** Core photo at Wolf that highlights the challenge of unravelling the gold history in metamorphosed deposits. Gold occurs within a tightly folded quartz (± ankerite) vein. S_{main} is axial planar to the folded vein; however, a late pyrrhotite-quartz-calcite fracture cuts the folded quartz veins and could be associated with the gold. **k)** Core photo of a deformed quartz-ankerite-gold vein cutting BIF at Tiriganiaq. A late pyrite-rich fracture cuts the auriferous quartz vein (abbreviations: Ank = ankerite; Aspy = arsenopyrite; BIF = banded iron formation; Chl = chlorite; lamp = lamprophyre; Po = pyrrhotite; Py = pyrite; Qtz = quartz).

contains pebble- to boulder-sized clasts comprising muscovite schist, quartzite, granodiorite/tonalite, and metabasalt hosted by a metasiltstone matrix (Fig. 3e). The polymictic conglomerate yields detrital zircon ages that range from 3.37 to 2.50 Ga, suggesting that this conglomerate was deposited ≤2.50 Ga and confirms that Paleoproterozoic, or younger, sedimentary successions are intercalated and folded with Neoarchean volcanic rocks comprising the Rankin Inlet greenstone belt (Davis et al., 2008). The second dated conglomerate comprises pebble- to cobble-sized clasts of quartzite and granodiorite/tonalite (Fig. 3f) and yields detrital zircon ages that range from 2.86 to

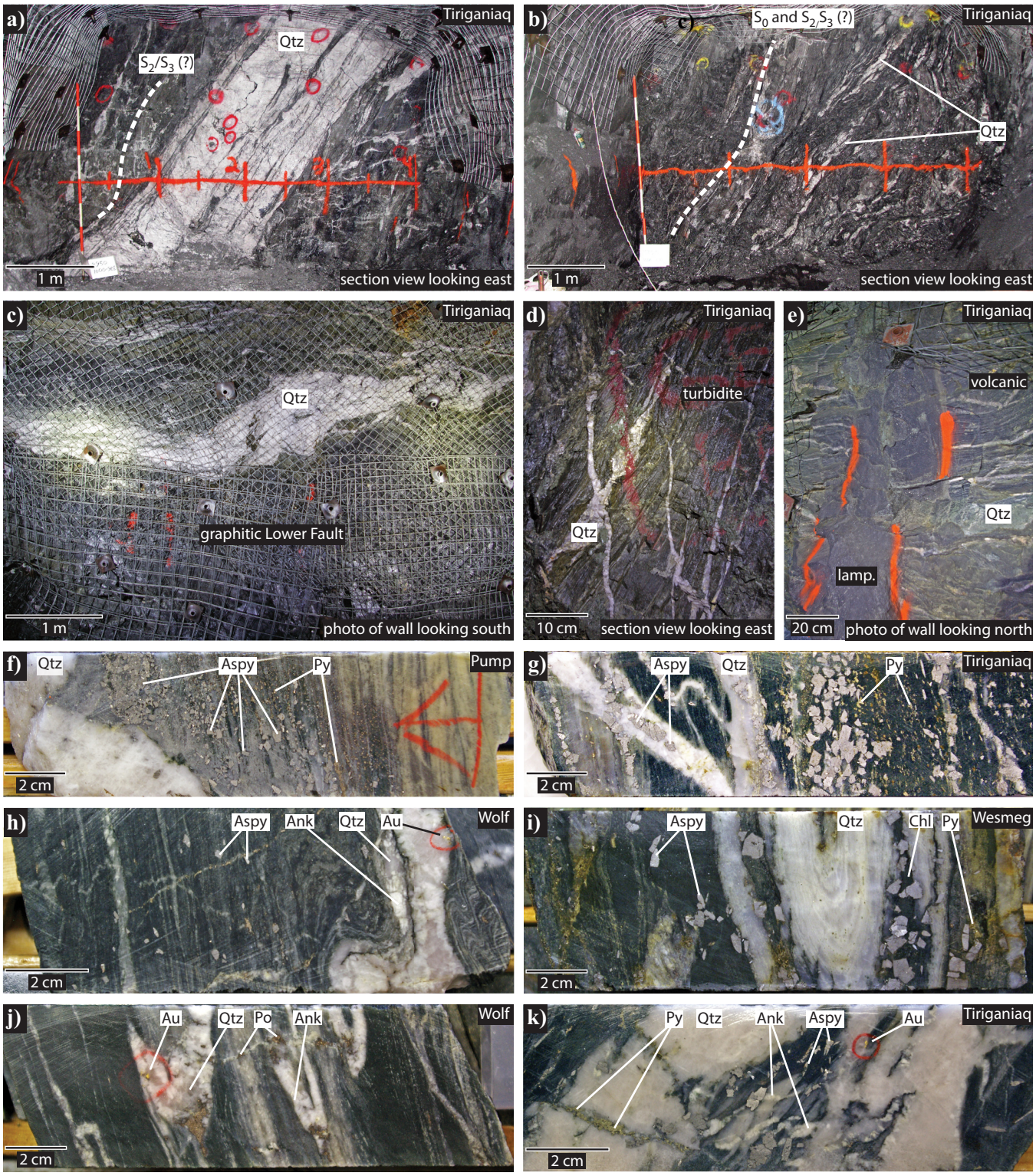

2.66 Ga, which suggests that this conglomerate was deposited at ≤2.66 Ga (Lawley et al., in prep).

Deposit U-Pb Xenotime Geochronology

Two auriferous quartz (± ankerite) vein samples cutting BIF and turbidite host rocks at Tiriganiaq were targeted for in situ U-Pb xenotime dating. Both samples were also dated via Re-Os arsenopyrite geochronology and compliment previously reported U-Pb monazite ages for the same deposit (Carpenter et al., 2005). Dated xenotime crystals postdate arsenopyrite (i.e. occur at arsenopyrite grain boundaries and fill arsenopyrite fractures) and yield a colinear array with an upper intercept Concordia age at 1862 ± 29 Ma (lower intercept = 117 ± 660 Ma; Mean Square Weighted Deviate, MSWD = 1.1; n = 15; 9 xenotime crystals). This upper intercept age is in excellent agreement with a weighted average $^{207}Pb/^{206}Pb$ age for all analyses at 1858 ± 10 Ma (MSWD = 1.1, n = 15; 9 xenotime crystals). Both age determinations are also in broad agreement with the previously reported preferred weighted mean $^{207}Pb/^{206}Pb$ monazite age at 1854 ± 6 Ma (MSWD = 1, n = 18; Carpenter et al., 2005). Undated ultrafine xenotime inclusions within arsenopyrite may represent an older, but undefined hydrothermal phosphate event(s) or could suggest that arsenopyrite crystals are locally ≤1.86 Ga.

Deposit Re-Os Arsenopyrite Geochronology

Arsenopyrite samples were collected from Tiriganiaq, Pump, F Zone, and Discovery. These samples share a similar paragenesis and occur with high-grade gold intervals at each of the targeted deposits (Fig. 4d–i). Gold fills arsenopyrite fractures and occurs at arsenopyrite crystal boundaries that, coupled with LA-ICP-MS in situ element mapping (Lawley et al., 2014a, b), provides evidence for late gold mobility and possible gold remobilization into low-strain microtextural sites. Arsenopyrite samples yield low Re-contents (0.5–6 ppb, n = 15) and are generally highly radiogenic (i.e. the Os isotopic composition is dominated by radiogenic ^{187}Os). Re-Os model ages range from 2.3 to1.8 Ga and point to complex Re-Os systematics that cannot be interpreted within the context of a single and cogenetic arsenopyrite sample suite. Replicate analyses of the two most Re-enriched samples yield the most uniform Re-Os model ages at 1899 ± 6 Ma (MSWD = 0.5, n =3) and 2269 ± 25 Ma (MSWD = 6, n = 5; Lawley et al., submitted a), respectively, whereas replicate analyses of Re-poor aliquots (≤1 ppb) yield variable Re-Os model ages between these two end-members.

We speculate that these homogeneous and reproducible Re-Os arsenopyrite ages are geologically meaningful and that arsenopyrite crystallization is significantly older than hydrothermal xenotime at ca. 1.86 Ga. If correct, new Re-Os ages are broadly concurrent with the Arrowsmith (2.4–2.3 Ga) and Snowbird (1.90 Ga) orogens (Berman et al., 2013) and record a hitherto unrecognized pre-1.86 Ga hydrothermal history at the MGD. Gold was likely introduced at ca. 2.27 and/or 1.90 Ga, whereas monazite and xenotime ages at ca. 1.86 Ga likely date phosphate and gold remobilization concomitant with the THO. Heterogeneous Re-Os arsenopyrite ages between 2.3 and 1.8 Ga could reflect partial open-system behaviour or mixing of disparate arsenopyrite generations that are evident from element mapping (Lawley et al., 2014b).

Hydrothermal Footprint

Fluid-rock interaction produces geochemical and mineralogical effects that can extend far beyond the economically viable portions of a hydrothermal ore deposit. This 'hydrothermal footprint' holds great promise as an exploration tool to vector from barren rock to high-grade gold ore and is a key tool in the search for new BIF-hosted gold deposits in metamorphosed and complexly deformed environments. As part of TGI-4 research at the MGD, we extended the probabilistic mapping approach, initially developed for geochemical survey studies, to hydrothermal footprint vectoring in the subsurface (Lawley et al., submitted b). Our conditional probability-based approach provides a framework to delineate domains of multivariate pathfinder-element enrichment and hydrothermally altered rock that extend 10s to 100s of meters beyond the gold ore zones. These anomalous domains occur in hanging wall and footwall rock devoid of gold (<5 ppb) and thus provide a possible vector to high-grade ore. At Tiriganiaq, hydrothermally altered and anomalous pathfinder-element concentrations extend for at least 200 m beyond the gold ore zone (Lawley et al., submitted b). We demonstrate that the accuracy and precision of portable X-Ray Fluorescence (pXRF) spectrometry on drill-core surfaces is sufficient to map multivariate hydrothermal footprints from the rock record in unprecedented detail and at a fraction of the cost and time compared to whole-rock analyses (Lawley et al., submitted b).

MULTISCALE IMPLICATIONS FOR EXPLORATION

Gold typically occurs in late fractures and other late and low-strain microtextural sites at orogenic deposits, which are the end-product of repeated hydrothermal stages linked to fluid-pressure cycling and episodic fluid infiltration in an active deformation zone (e.g. the fault-valve model; Sibson et al., 1988). Gold is expected to precipitate in multiple stages throughout this complex hydrothermal and deformation history and yet it typically occurs as the latest mineral phase at the microscale. This classic ore texture is the subject of

continued controversy and has been taken as evidence for (1) the relatively late timing for the bulk of the gold; (2) remobilized gold that was liberated from early and gold-rich sulphides and then redistributed during later fluid-assisted metamorphic and/or structural events; and/or (3) a mixture of these processes. Each scenario requires a tailored mineral exploration strategy and thus the absolute age of gold represents a key uncertainty for mineral explorationists. In the case of metamorphosed deposits, the current textural setting of gold is of great importance for defining deposit-scale ore shoots, but it likely reveals very little on how gold was initially introduced, which has major impacts on local- to regional-scale exploration models.

The late gold paragenesis at the MGD, coupled with U-Pb hydrothermal monazite ages at ca. 1.85 Ga, led to an inferred late gold model and a genetic link with the THO (1.9–1.8 Ga). Critically, the previous gold model implied that (1) MGD auriferous quartz veins are relatively undeformed; (2) idioblastic arsenopyrite crystals associated with gold are late and largely postdate the main regional foliation; and (3) late D_3 structures are prospective for gold, whereas D_2 folding and thrusting predate gold and thus were considered unprospective (Carpenter and Duke, 2004; Carpenter et al., 2005). Tiriganiaq and Pump are associated with D_3 east-trending shearing and Z-folding, respectively, and thus represent type examples of the late gold model (Fig. 1).

The link between gold and late reworking at the MGD is also supported by recent studies at other BIF-hosted gold deposits within the WCP (e.g. Three Bluffs, Davies et al., 2010; Meadowbank, Sherlock et al., 2004). Each of these studies proposed a genetic link between gold and the THO. This tectono-thermal event represents the latest Paleoproterozoic orogenic phase that is recorded across large swaths of the WCP. Accordingly, the Trans-Hudson Paleoproterozoic Metallotect has been tentatively correlated from northern Nunavut to Saskatchewan and Manitoba (e.g. Davies et al., 2010). In contrast, the gold fertility and prospectivity of orogenic episodes and fault-networks that predate the THO were undemonstrated.

Reproducible replicate analyses of the two most Re-rich samples yield the least evidence for disturbance and potentially record a pre-1.86 Ga gold-bearing sulphide history. If correct, arsenopyrite crystals may have initially crystallized concomitant with the Arrowsmith and/or Snowbird orogenies along with early arsenopyrite (i.e. 2.27 and/or 1.90 Ga). Gold was likely introduced along with early arsenopyrite and then remobilized during the later stages of the THO (i.e. 1.86–1.85 Ga). Late gold enrichment is also demonstrated by in situ LA-ICP-MS trace element mapping and spot analyses (Lawley et al., 2014b).

Idioblastic arsenopyrite crystals are also concentrated at the margins and within the halo of folded and transposed auriferous quartz (± ankerite) veins at each of the studied deposits. At Tiriganiaq, the main auriferous quartz vein, which occurs along the Lower Fault and shares similarities with fault-fill veins, is folded, boudinaged, and transposed subparallel to S_{main} (Fig. 4a, c). Smaller scale quartz (± ankerite) veins are also tightly folded and transposed subparallel to S_{main} in Tiriganiaq hanging wall and footwall rocks (Fig. 4b, d). Dated arsenopyrite crystals within and at the margins of these veins are wrapped by the bedding-parallel fabric and locally contain quartz strain fringes that point to post-crystallization strain across the MGD. These field and core observations at Tiriganiaq and the other deposits are at odds with the late gold metallogenic model proposed by Carpenter et al. (2005).

The 'early' gold model proposed here suggests that the Proterozoic Gold Metallotect as defined by Miller et al. (1994) in fact comprises several temporally distinct gold-bearing events. Differentiating between these events represents a critical step for effective mineral exploration. For example, the geometry of gold deposits is likely to have undergone variable degrees of structural reworking dependent, in part, on their timing relative to the WCP's polyorogenic Paleoproterozoic history and the extent of structural reactivation during each orogenic phase.

In the case of the MGD, the suggested pre-1.86 Ga hydrothermal and deformation history likely represent key factors in understanding the current geometry and occurrence of gold at the MGD, but are obscured by overprinting metamorphic/hydrothermal/deformation events related to the later stages of the THO. A metamorphosed, folded, and transposed gabbroic dyke at Discovery (Fig. 3h) contains metamict zircons that have been dated at ca. 1.81 Ga, which likely record the timing of metamorphism or a hydrothermal event, as opposed to its emplacement age. Undeformed lamprophyre dykes cut the main deposit fabric and folded quartz veining at Tiriganiaq (Fig. 4e) and, if correlative with the ca. 1.833 Ga Christopher Island Formation (Rainbird et al., 2006), provide a minimum age for the main deposit fabric (Carpenter and Duke, 2004; Carpenter et al., 2005). The deformed ≤2.155 Ga conglomerate south of the Pyke Fault further supports reworking from 2.155 to 1.833 Ga (Davis et al., 2008).

The MGD thus represents one of the few global examples of Proterozoic gold hosted at a reworked Archean cratonic margin. This geodynamic setting is distinct from classic orogenic gold deposits, which are hosted by Neoarchean granite-greenstone terranes that are broadly coeval (e.g. 10s Myr; Dubé and Gosselin, 2007) with auriferous fluids and spatially associated with terrane-bounding faults. At these deposits, gold is

intricately linked to basin development and subsequent reactivation during crustal shortening is linked to convergent tectonics and consanguineous metamorphism. An important corollary to this observation is that Neoarchean greenstone belts are also favourable gold exploration targets after reworking during much younger and overprinting tectono-thermal events. We consider that Archean basins, once formed, provide a crustal architecture (ground preparation) that facilitates subsequent reactivation and thus Archean fault networks represent zones of long-lived structural weakness. Archean basins in the WCP also comprise favourable host-rocks (e.g. mafic volcanic rocks, turbidite sequences, and BIF) that differ from granitoids and Proterozoic basins, which are comparatively gold-poor in the WCP. Together these apparent structural and lithostratigraphic gold controls likely contribute to the similar setting of Paleoproterozoic WCP gold districts to their Archean equivalents.

ACKNOWLEDGEMENTS

The MGD study is conducted under the auspices of Natural Resource Canada's Targeted Geoscience Initiative (TGI)-4. The authors would like to thank the cooperation and input from Agnico-Eagle Mines Ltd. throughout the study period. In particular, Denis Vaillancourt, Robert Fraser, Jérôme Lavoie, and Francine Fallara are thanked for sharing their knowledge and facilitating fieldwork logistics, assisting on site, and providing unpublished assays results, borehole logs, and geological plans/sections for the studied deposits.

REFERENCES

Aspler, L.B., and Chiarenzelli, J.R., 1996. Stratigraphy, sedimentology and physical volcanology of the Henik Group, central Ennadai-Rankin greenstone belt, Northwest Territories, Canada: Late Archean paleogeography of the Hearne Province and tectonic implications; Precambrian Research, v. 77, p. 59–89.

Bannatyne, M.J., 1958. The Geology of the Rankin Inlet Area and North Rankin Nickel Mines Limited, Northwest Territories; M.Sc. Thesis, University of Manitoba, Winnipeg, Manitoba.

Berman, R.G., Davis, W.J., and Pehrsson, S., 2007. The collisional Snowbird tectonic zone resurrected: Growth of Laurentia during the 1.9 Ga accretionary phase of the Trans-Hudson orogeny; Geology, v. 35, p. 911–914.

Berman, R.G., Pehrsson, S., Davis, W.J., Ryan, J.J., Qui, H., and Ashton, K.E., 2013. The Arrowsmith orogeny: Geochronological and thermobarometric constraints on its extent and tectonic setting in the Rae craton, with implications for pre-Nuna supercontinent reconstruction; Precambrian Research, v. 232, p. 44–69.

Carpenter, R.L. and Duke, N.A., 2004. Geological setting of the West Meliadine Gold Deposits, Western Churchill Province, Nunavut, Canada; Exploration and Mining Geology, v. 13, p. 49−65.

Carpenter, R.L., Duke, N.A., Sandeman, H.S., and Stern, R., 2005. Relative and absolute timing of gold mineralization along the Meliadine Trend, Nunavut, Canada: Evidence for Paleoproterozoic gold hosted in an Archean greenstone belt; Economic Geology, v. 100, p. 567−576.

Davies, T., Richards, J.P., Creaser, R., Heaman, L.M., Chacko, T., Simonetti, A., Williamson, J., and McDonald, D.W., 2010. Paleoproterozoic age relationships in the Three Bluffs Archean iron-formation-hosted gold deposits, Committee Bay Greenstone Belt, Nunavut, Canada; Exploration and Mining Geology, v. 19, p. 55–80.

Davis, W.J. and Miller, A.R., 2001. A Late Triassic Rb-Sr phlogopite isochron age for a kimberlite dyke from the Rankin Inlet area, Nunavut; Geological Survey of Canada, Radiogenic Age and Isotopic Studies Report 14, Current Research 2001-F3, 5 p.

Davis, W.J., Ryan, J.J., Sandeman, H.A., and Tella, S., 2008. A Paleoproterozoic detrital zircon age for a key conglomeratic horizon within the Rankin Inlet area, Kivalliq Region, Nunavut: Implications for Archean and Proterozoic evolution of the area; Geological Survey of Canada, Current Research 2008-8, 8 p.

Dubé, B. and Gosselin, P., 2007. Greenstone-hosted quartz-carbonate vein deposits, *In:* Mineral Deposits of Canada: A Synthesis of Major Deposit Types, District Metallogeny, the Evolution of Geological Provinces, and Exploration Methods, (ed.) W.D. Goodfellow; Geological Association of Canada, Mineral Deposits Division, Special Publication no. 5, p. 49–73.

Dubé, B., Mercier-Langevin, P., Castonguay, S., McNicoll, V.J., Pehrsson, S.J., Bleeker, W., Schetselaar, E.M., and Jackson, S., 2011. Targeted Geoscience Initiative 4. Lode gold deposits in ancient, deformed and metamorphosed terranes – footprints and exploration implications: A preliminary overview of themes, objectives and targeted areas, *In:* Summary of Field Work and other Activities 2011; Ontario Geological Survey, Open File Report 6270, p. 38-1 to 38-10.

Hoffman, P.F., 1988. United plates of America, the birth of a craton: Early Proterozoic assembly and growth of Laurentia; Annual Review of Earth and Planetary Sciences, v. 16, p. 543–603.

Lawley, C.J.M., Creaser, R.A., McNicoll, V., Dubé, B., Mercier-Langevin, P., Pehrsson, S., and Vaillancourt, D., 2014a. Re-Os arsenopyrite and U-Pb detrital zircon geochronology at the Meliadine Gold District, Nunavut: Implications for the geologic setting and age of the Tiriganiaq Deposit; Geological Survey of Canada, Open File 7510, 19 p. doi:10.4095/293939

Lawley, C.J.M., Dubé, B., Jackson, S., Yang, Z., Mercier-Langevin, P., and Vaillancourt, D., 2014b. Sulfide paragenesis and LA-ICP-MS arsenopyrite geochemistry at the Meliadine Gold District, Nunavut: Implications for Re-Os arsenopyrite geochronology and ore deposit genesis; Geological Survey of Canada, Open File 7491, 1 poster. doi:10.4095/293938

Lawley, C.J.M., Creaser, R., Jackson, S., Yang, Z., Davis, B., Pehrsson, S., Dubé, Mercier-Langevin, P., and Vaillancourt, D., submitted a. Unravelling the Western Churchill Province Paleoproterozoic Gold Metallotect: Constraints from Re-Os arsenopyrite and U-Pb Xenotime Geochronology and LA-ICP-MS arsenopyrite geochemistry at the BIF-Hosted Meliadine Gold District, Nunavut, Canada; Economic Geology.

Lawley, C.J.M., Dubé, B., Mercier-Langevin, P., Kjarsgaard, B., Knight, R., and Vaillancourt, D., submitted b. Defining and mapping hydrothermal footprints at the BIF-hosted Meliadine Gold District, Nunavut, Canada; Journal of Geochemical Exploration.

Lawley, C.J.M., McNicoll, V., Castonguay, S., Dubé, B., Mercier-Langevin, P., Pehrsson, S., in prep. Geology of the Meliadine Gold District.

Miller, A.R., Balog, M.J., Barham, B.A., and Reading, K.L., 1994. Geology of the Early Proterozoic gold metallotect, Hurwitz Group in the Cullaton-Griffin lakes area, central Churchill

Structural Province, Northwest Territories, *In:* Current Research 1994-C; Geological Survey of Canada, p. 135–146.

Miller, A.R., Balog, M.J., and Tella, S., 1995. Oxide iron-formation-hosted lode gold, Meliadine trend, Rankin Inlet Group, Churchill Province, Northwest Territories, *In:* Current Research 1995-C; Geological Survey of Canada, p. 163–174.

Pehrsson, S.J., Berman, R.G., and Davis, W.J., 2013a. Paleoproterozoic orogenesis during Nuna aggregation: A case study of reworking of the Rae craton, Woodburn Lake, Nunavut; Precambrian Research, v. 232, p. 167–188.

Pehrsson, S.J., Berman, R.G., Eglington, B., and Rainbird, R., 2013b. Two Neoarchean supercontinents revisited: The case for a Rae family of cratons; Precambrian Research, v. 232, p. 27–43.

Rainbird, R.H., Davis, W.J., Stern, R.A., Peterson, T.D., Smith, S.R., Parrish, R.R., and Hadlari, T., 2006. Ar-Ar and U-Pb geochronology of a late Proterozoic rift basin: Support for a genetic link with Hudsonian orogenesis, western Churchill Province, Nunavut, Canada; The Journal of Geology, v. 114, p. 1–17.

Sherlock, R., Pehrsson, S., Logan, A.V., Hrabi, R.B., and Davis, W.J., 2004. Geological setting of the Meadowbank Gold Deposits, Woodburn Lake Group, Nunavut; Exploration and Mining Geology, v. 13, p. 67–107.

Sibson, R.H., Robert, F., and Poulsen, K.H., 1988. High-angle reverse faults, fluid-pressure cycling, and mesothermal gold-quartz deposits; Geology, v. 16, p. 551-555.

Tella, S., Mikkel, S., Armitage, A.E., Seemayer, B.E., and Lemkow, D., 1992. Precambrian geology and economic potential of the Meliadine Lake-Barbour Bay region, district of Keewatin, Northwest Territories, *In:* Current Research, Part C; Geological Survey of Canada, Paper 92-1C, p. 1–11.

Tella, S., Roddick, J.C., and van Breemen, O., 1996. U-Pb zircon age for a volcanic suite in the Rankin Inlet Group, Rankin Inlet map area, District of Keewatin, Northwest Territories; Geological Survey of Canada, Radiogenic Age and Isotopic Studies Report 9, p. 11–15.